Variability in QBO Temperature Anomalies on Annual and Decadal Time Scales

ZANE MARTIN,[a] ADAM SOBEL,[b,c] AMY BUTLER,[d] AND SHUGUANG WANG[b]

[a] *Department of Atmospheric Science, Colorado State University, Fort Collins, Colorado*
[b] *Department of Applied Physics and Applied Mathematics, Columbia University, New York, New York*
[c] *Lamont-Doherty Earth Observatory of Columbia University, Palisades, New York*
[d] *NOAA/Chemical Sciences Laboratory, Boulder, Colorado*

(Manuscript received 22 April 2020, in final form 7 October 2020)

ABSTRACT: The stratospheric quasi-biennial oscillation (QBO) induces temperature anomalies in the lower stratosphere and tropical tropopause layer (TTL) that are cold when lower-stratospheric winds are easterly and warm when winds are westerly. Recent literature has indicated that these QBO temperature anomalies are potentially important in influencing the tropical troposphere, and particularly in explaining the relationship between the QBO and the Madden–Julian oscillation (MJO). The authors examine the variability of QBO temperature anomalies across several time scales using reanalysis and observational datasets. The authors find that, in boreal winter relative to other seasons, QBO temperature anomalies are significantly stronger (i.e., colder in the easterly phase of the QBO and warmer in the westerly phase of the QBO) on the equator, but weaker off the equator. The equatorial and subtropical changes compensate such that meridional temperature gradients and thus (by thermal wind balance) equatorial zonal wind anomalies do not vary in amplitude as the temperature anomalies do. The same pattern of stronger on-equatorial and weaker off-equatorial QBO temperature anomalies is found on decadal time scales: stronger anomalies are seen for 1999–2019 compared to 1979–99. The causes of these changes to QBO temperature anomalies, as well as their possible relevance to the MJO–QBO relationship, are not known.

KEYWORDS: Quasibiennial oscillation; Madden-Julian oscillation; Stratosphere-troposphere coupling; Decadal variability; Seasonal cycle; Seasonal variability

1. Introduction

The tropical tropopause layer (TTL; Fueglistaler et al. 2009) delineates the boundary between the troposphere and stratosphere. The TTL is crucial for setting the water budget of the stratosphere, has implications for ozone chemistry and tracer movement, and exhibits strong signatures of anthropogenic warming (Fueglistaler et al. 2009; Lin et al. 2017). Existing literature has further established that TTL temperatures undergo strong variations on many time scales: they show a strong annual cycle (Gettelman and de Forster 2002; Jucker and Gerber 2017) and are further impacted by tropospheric and stratospheric modes of variability, including the Madden–Julian oscillation (MJO; Madden and Julian 1971, 1972, 1994; Zhang 2005; Son and Lee 2007; Virts and Wallace 2014), the stratospheric quasi-biennial oscillation (QBO; Baldwin et al. 2001; Huesmann and Hitchman 2001), and El Niño–Southern Oscillation (ENSO; Domeisen et al. 2019).

The study of TTL temperatures has recently been reinvigorated by the discovery of a strong relationship between the QBO and the MJO (Yoo and Son 2016; Son et al. 2017; Nishimoto and Yoden 2017). The QBO phase accounts for roughly 50% of the interannual variation in MJO strength during boreal winter with a stronger MJO when the QBO winds (at 50 hPa) are easterly and the TTL is anomalously cold (Son et al. 2017). In addition to modulating the strength of the MJO, the QBO also alters the behavior and predictability of MJO teleconnections (Mundhenk et al. 2018; Mayer and Barnes 2020; Hera Kim et al. 2020; Toms et al. 2020), and may enhance MJO predictability (Marshall et al. 2017; Lim et al. 2019; Wang et al. 2019; Kim et al. 2019). A clear mechanism linking the MJO and QBO has not been established, but an increasing body of work suggests that TTL temperature anomalies may be a primary cause (Nie and Sobel 2015; Yoo and Son 2016; Son et al. 2017; Hendon and Abhik 2018; Klotzbach et al. 2019; Abhik et al. 2019; Martin et al. 2019, 2020).

The most likely explanation for the observed and simulated relationships between TTL temperature and MJO amplitude is that colder TTL temperatures, such as those experienced in the easterly phase of the QBO (QBOE), allow convection to penetrate deeper into the troposphere more vigorously, whereas warmer TTL temperatures in the westerly phase of the QBO (QBOW) have the opposite effect. MJO convection may be particularly affected because is generally extensive, deep, and vertically coherent, and is able to reach the level of QBO influence (Hendon and Abhik 2018). However, the precise details of this destabilization have not been fully articulated or agreed upon as key to the MJO–QBO link, and are difficult to capture in global climate models (Lee and Klingaman 2018; Hyemi Kim et al. 2020).

In an idealized cloud-resolving model, Martin et al. (2019) showed that imposing anomalous temperatures in the upper troposphere and stratosphere could affect MJO convection in a manner qualitatively consistent with observations. However, that study found it necessary to impose temperature anomalies larger and lower than those observed to produce clear changes to MJO convection. The MJO convective response to QBO-like

Corresponding author: Zane Karas Martin, zkmartin@rams.colostate.edu

DOI: 10.1175/JCLI-D-20-0287.1

temperature anomalies was sensitive to the precise structure of imposed temperature anomalies around the TTL, and larger-amplitude temperature anomalies were linked to stronger MJO responses.

Whether the TTL temperature mechanism is key for the MJO–QBO connection is still unsettled. However, if this mechanism is operative there are two key features of the MJO–QBO link it ought to explain: the seasonality and the long-term trend. On annual time scales, the MJO–QBO link is only statistically significant in boreal winter (December–February; Yoo and Son 2016). On longer time scales, Klotzbach et al. (2019) showed that the MJO–QBO relationship has changed over the course of the twentieth century, with the lack of a connection prior to the 1980s and emergence of a link only in recent decades. Inspired by those studies, here we examine TTL temperature signals associated with the QBO on interannual, annual, and decadal time scales.

This study is organized as follows: section 2 describes reanalysis and observational data we use to characterize TTL temperatures, the indices used to track various climate processes, and additional methodological details. Section 3 presents our results: the first subsection examines TTL temperature signals generally, the second examines how QBO temperature anomalies change with the annual cycle, and the third considers QBO temperatures on decadal time scales. In section 4 we discuss hypothetical mechanisms related to our findings. Section 5 summarizes this study.

2. Data and indices

a. Data

We make use of five reanalysis products, radiosonde observations from one site, and a dataset of reanalysis-derived zonal-mean diagnostics of the residual circulation. The consistency of our results across several datasets is an indicator of the robustness of our findings. The data span roughly the period from 1 January 1979 to 31 December 2018, or as close to that period as possible given each product's availability. Additionally, one reanalysis product (JRA-55, defined below) and the sounding data were examined starting from 1 January 1958. Recent initiatives using most of the reanalysis datasets we consider, including especially the SPARC Reanalysis Intercomparison Project (S-RIP; Fujiwara et al. 2017), have examined the commonalities and differences in the representation of the stratosphere and upper troposphere across reanalysis products. Results have shown that the modern reanalysis products considered here provide a good representation of TTL temperatures compared to observations (Tegtmeier et al. 2020).

The reanalysis products we consider are the NCEP–NCAR Reanalysis 1 (R1; Kalnay et al. 1996; Kistler et al. 2001), ERA-5 (Hersbach et al. 2019), NASA's Modern-Era Retrospective Analysis for Research and Applications 2 (MERRA-2; Gelaro et al. 2017), and the Japanese 55-year Reanalysis Project (JRA-55; Kobayashi et al. 2015). In addition to JRA-55, we also utilize "JRA-55C" (Kobayashi et al. 2014) through 2012 (due to availability), which is identical to JRA-55 except that it excludes satellite data in its data assimilation. This allows one to examine whether particular features in the standard JRA-55 are attributable to changes in observing systems. We use monthly mean data, as well as daily data from MERRA-2 and ERA5.

In addition to reanalysis, we use monthly and daily data from the Singapore sounding station, located at approximately 1°N, 104°E. Singapore was chosen because it has been a hallmark of QBO studies and has a long record of available data. Sounding data were retrieved through the Integrated Global Radiosonde Archive, version 2 (Durre et al. 2006; Durre and Yin 2008).

In section 4, we analyze the stratospheric zonal-mean residual circulation as computed via the transformed Eulerian-mean (TEM) framework (Andrews et al. 1987; Salby 1996), as well as the Eliassen–Palm (EP) flux divergence. The residual circulation, whose meridional and vertical components are denoted v^* and w^* (or ω^* in pressure coordinates), represents the combined effects of both eddy and mean transport in the circulation. Among many other applications, the TEM framework, residual circulation, and EP flux have proven useful for understanding the Brewer–Dobson circulation [BDC; for review see Butchart (2014)], a planetary-scale overturning circulation that spans the stratosphere.

A dataset that includes v^* and ω^* values and EP flux quantities from 14 major reanalysis products (as well as other TEM and further diagnostics quantities) has been made available publicly as part of the S-RIP project [Martineau 2017; see details in Martineau et al. (2018)]. Readers are referred to Martineau et al. (2018) for additional details regarding the precise formulation and calculation of these quantities and details on the dataset. From the full dataset, we utilized v^* and ω^* values (converted to w^*) and the EP-flux divergence from ERA-Interim (Dee et al. 2011). The diagnostics are available on both each reanalysis product's original grid and a common grid; we use the common grid product. We utilized monthly-mean data from January 1980 to December 2016.

More details regarding the horizontal, vertical, and temporal resolution of the datasets we consider can be found in Table 1.

b. MJO, QBO, and ENSO indices

We track the MJO using the daily Real-time Multivariate MJO index (RMM; Wheeler and Hendon 2004). RMM is a standard MJO index formed using the leading pair of EOFs of OLR and zonal wind anomalies at 850 and 200 hPa averaged over the tropics, which are projected onto the EOFs to form two principal component time series: RMM1 and RMM2. RMM1 and RMM2 track the strength and location of the MJO: their phase angle represents the MJO's location, and the amplitude ($\sqrt{\text{RMM1}^2 + \text{RMM2}^2}$) represents the MJO's strength. We use the observed RMM index available from the Australian Bureau of Meteorology. We do not recalculate RMM for various reanalysis products. We define strong and weak MJO months as periods when the monthly mean RMM amplitude is, respectively, greater than or less than one-half standard deviation above or below the mean. This threshold is defined independent of month or season, as discussed more in section 3a.

To track ENSO we use the Hadley Centre Niño-3.4 index, formed by monthly averaging SST anomalies between 5°N and 5°S and between 170° and 120°W. El Niño events are defined

TABLE 1. List of data products used in this study, as discussed in section 2. Spatial resolution is given horizontally, followed by the vertical levels retrieved (in hPa). Not all available vertical levels were retrieved for all products, but the highest available resolution was selected in the TTL. S-RIP diagnostics are from the datasets described in section 2 and in Martineau et al. (2018).

Name	Type	Spatial resolution	Temporal resolution
R1	Reanalysis	2.5° × 2.5° 17 vertical levels: 1000, 925, 850, 700, 600, 500, 400, 300, 250, 200, 150, 100, 70, 50, 30, 20, 10 hPa	Monthly Jan 1979–Dec 2018
ERA5	Reanalysis	1° × 1° 22 vertical levels: 1000–800 hPa by 50 hPa; 800–300 hPa by 100 hPa; 250–100 hPa by 25 hPa; 70, 50, 30, 20, 10 hPa	Monthly and daily Jan 1979–Dec 2018
MERRA-2	Reanalysis	1° × 1° 19 vertical levels: 1000–800 hPa by 50 hPa; 800–200 hPa by 100 hPa; 150, 100, 70, 50, 40, 30, 20, 10 hPa	Monthly and daily Jan 1980–Dec 2018
JRA-55	Reanalysis	2.5° × 2.5° 18 vertical levels: 1000–800 hPa by 50 hPa; 800–200 hPa by 100 hPa; 150, 100, 70, 50, 30, 20, 10	Monthly Jan 1958–Dec 2018
JRA-55C	Reanalysis	2.5° × 2.5° 18 vertical levels: 1000–800 hPa by 50 hPa; 800–200 hPa by 100 hPa; 150, 100, 70, 50, 30, 20, 10	Monthly Jan 1958–Dec 2012
Singapore	Sounding	17 vertical levels: Surface, 1000, 925, 850, 700, 500, 400, 300, 250, 200, 150, 100, 70, 50, 30, 20, 10 hPa	Monthly and daily Jan 1958–Dec 2018
ERA-Interim	S-RIP diagnostics	Zonal mean; 2.5° latitude 6 vertical levels: 100, 70, 50, 30, 20, 10 hPa	Monthly Jan 1980–Dec 2016

when the index value is greater than one standard deviation, and La Niña events are defined when the value is less than minus one standard deviation.

To track the QBO we use the monthly-mean 50-hPa zonal-mean zonal wind, averaged between 10°N and 10°S in each dataset (U50). As in previous studies (e.g., Yoo and Son 2016; Son et al. 2017) we define westerly and easterly QBO phases as months when the index is, respectively, greater than or less than one-half standard deviation above or below the mean. For the Singapore sounding data, we use the value of the monthly-mean Singapore zonal wind at 50 hPa.

Figure 1 shows the QBO index from all datasets and shows very good agreement representing the QBO. The correlation between each reanalysis dataset and ERA5 is over 0.99. The correlation between JRA-55 and JRA-55C is approximately 0.998, suggesting that changes in observing systems do not have a large impact on monthly 50-hPa winds. The Singapore U50 index (black line in Fig. 1) is noisier than the reanalyses and has greater maxima or lesser minima during some QBO peaks (although the correlation with ERA5 is still high: ~0.97). This is in part due to the tropical averaging in the reanalysis calculations that smooths variability associated with a single point and includes averaging over off-equatorial

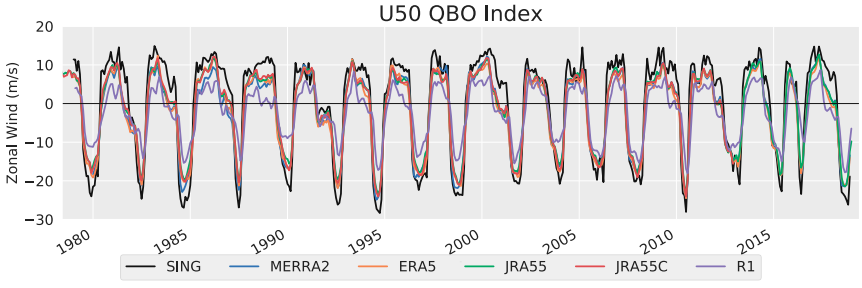

FIG. 1. The monthly U50 QBO index (zonal-mean zonal wind at 50 hPa averaged over 10°N to 10°S) for all datasets. For Singapore, no spatial averaging is possible so monthly values at 50 hPa are used. The period shown (1979–2018) corresponds to the period over which most datasets overlap, although JRA-55 and JRA-55C extend back to 1958.

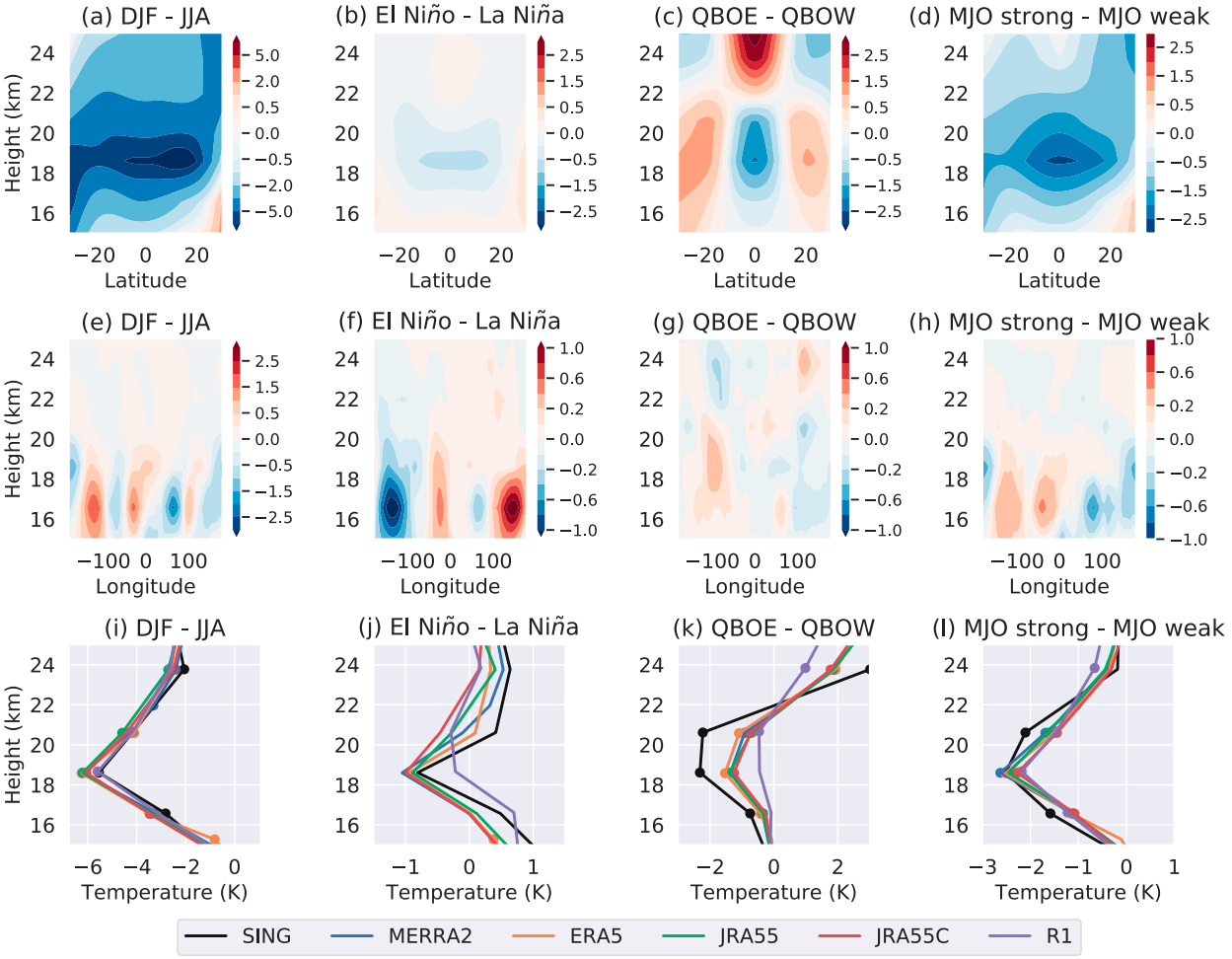

FIG. 2. (a)–(d) MERRA-2 zonal-mean temperature differences between (left to right) December–February and June–August periods, El Niño and La Niña periods, QBOE and QBOW periods, and strong and weak MJO periods as defined in section 2. (e)–(h) MERRA-2 anomalies for the 10°N–10°S-averaged zonal anomaly relative to the zonal mean. (i)–(l) The tropical mean (zonally and 10°N–10°S averaged) differences, with lines showing all datasets as defined in the legend and Table 1. Levels that are statistically significant via a bootstrapping methodology (section 2) are dotted.

latitudes. The R1 reanalysis is also an outlier in that it tends to underestimate the strength of the QBO, with amplitudes at times 5–10 $\mathrm{m\,s^{-1}}$ smaller than other datasets. Overall however, the period and timing of QBO transitions look similar in all datasets.

In section 4, we identify QBO easterly and westerly peaks in these U50 time series. This is done by first identifying local extrema in QBOE and QBOW: for QBOE these minima are defined as those times t such that $\mathrm{U50}(t-1) > \mathrm{U50}(t)$ and $\mathrm{U50}(t) < \mathrm{U50}(t+1)$ (and similarly for QBOW with the sign changed to identify maxima). We further require that the QBOE peaks are less than $-14\,\mathrm{m\,s^{-1}}$ and the QBOW peaks are greater than $5\,\mathrm{m\,s^{-1}}$ in magnitude; these thresholds were chosen so that the identified extrema corresponded with those obvious by eye in the data. Finally, we required that the QBOE and QBOW peaks be separated by 20 months.

Finally, to test statistical significance throughout this study we utilize bootstrapping tests to determine whether the difference between two subsets of data is significant. For two generic subsets with sample size N_1 and N_2, this is done by first selecting N_1 and N_2 data points randomly without replacement from all available data, and then differencing these two random subsets. We repeat this process 1000 times to build up a distribution and assess significance at the 95% confidence level. All bootstrapping tests follow this general methodology; more specific details of our testing methodology in particular instances are further given in section 3.

3. Results

a. TTL variability across time scales

The QBO, annual cycle, ENSO, and the MJO all contribute to variability in TTL temperatures. Figure 2 shows the difference in TTL temperatures formed by compositing onto different phases of the four modes of variability we consider: for the annual cycle we take winter minus summer; for ENSO we take El Niño minus La Niña; for the QBO we take QBOE minus QBOW; and for the MJO we subtract strong and weak MJO months. The top two

rows show, respectively, the zonal-mean difference and the zonal anomalies averaged from 10°N to 10°S relative to the zonal-mean difference from MERRA-2. The bottom row shows the tropical (i.e., zonal and 10°N–10°S mean) differences for all datasets; significance via the bootstrapping method described in section 2 was conducted at each vertical level, and significant points are marked with a dot in Figs. 2i–l.

It is clear from Fig. 2 that the annual cycle, ENSO, the QBO, and the MJO all influence TTL temperatures. The TTL is colder in northern winter than in northern summer, as is well known (e.g., Fueglistaler et al. 2009, and older citations therein) though still not entirely well understood (Randel and Jensen 2013; Jucker and Gerber 2017). The TTL is also colder during QBOE than QBOW, consistent with thermal wind balance given the differences in zonal wind that define QBOE and QBOW (assuming constant meridional structure). For both the annual cycle and QBO zonal mean signals are relatively large (Figs. 2a,c) and show small zonal asymmetries (Figs. 2e,g).

In the case of ENSO, the zonal mean indicates relatively weak and insignificant TTL cold anomalies in El Niño relative to La Niña (Fig. 2b). However, this small zonal-mean signature is the cancellation of two larger terms (Fig. 2f): there are larger cold anomalies centered over the east Pacific and warm anomalies approximately over the west Pacific [noted for example in Domeisen et al. (2019)]. Note that these temperature changes are consistent with the changes in tropospheric convection caused by ENSO: the TTL is coldest above the enhanced convection in the eastern Pacific during El Niño.

The MJO signal in Fig. 2d appears quite strong, but much of this is an artifact of aliasing. The MJO is strongest in boreal winter (e.g., Zhang 2005) and is stronger in QBOE relative to QBOW (e.g., Son et al. 2017). Thus, the cold anomaly in the TTL in Fig. 2d is due to sampling bias: strong MJO months correspond to TTL states taken preferentially in winter and during QBOE, whereas weak MJO months are typically in summertime and QBOW. We confirmed this explanation by recalculating MJO differences restricting our analysis to only certain seasons and QBO phases (not shown). This reduces the TTL anomalies substantially: anomalies at upper levels on the equator around 18 km are found to be less than 1 K.

Figures 2i–l show results from all the datasets considered. Overall, the results are comparable in all datasets to the top panels in terms of the structure and magnitude of the temperature anomalies, although some diversity among datasets is seen. The Singapore and R1 products have smaller annual cycle magnitudes than do the other sources. In the sounding data this appears to be in part due to the lack of meridional and zonal averaging, which we confirmed by subsampling the MERRA-2 data at approximately the same point as Singapore (i.e., taking reanalysis values only at approximately 1°N, 104°E). This increases the similarity between these two datasets (not shown), although the reanalysis difference in the annual mean is still somewhat larger than the sounding data by approximately 0.5 K for unknown reasons.

The weak R1 signal is consistent with its behavior in general: it displays a weaker ENSO signal that peaks at higher levels than other datasets, as well as an almost nonexistent QBO temperature change. Other studies have noted deficiencies of this dataset's representation in particular of QBO temperature signals (Tegtmeier et al. 2020) and have attributed issues to the low vertical resolution and the use of poorly resolved satellite temperature retrievals (Fujiwara et al. 2017; Tegtmeier et al. 2020).

Other reanalysis datasets agree well with regard to ENSO and QBO anomalies. The QBO anomalies are stronger in the Singapore soundings than the reanalyses, which we again attribute to the lack of zonal and meridional averaging and with the stronger wind anomalies noted in Fig. 1. As previously, this was confirmed by subsampling MERRA-2 data from near the Singapore location, which leads to very similar QBO and ENSO anomalies between the reanalysis and sounding data. For the MJO, the datasets agree quite well, although the same aliasing issues noted above still hold.

Having established that the four climate processes discussed above can impact the TTL, next we examine the variability in QBO temperature anomalies across the intraseasonal to interannual time scales on which these various processes operate.

b. *QBO boreal winter temperature anomalies*

In this subsection we examine whether QBO temperature anomalies are stronger in boreal winter than other seasons, and how the annual cycle and the QBO interact. Figure 3 shows zonal-mean QBO anomalies in boreal winter versus those taken irrespective of season. The top row is similar to Fig. 2c (Fig. 3a is identical) and shows the QBOE minus QBOW temperature difference independent of season (Figs. 3a,c) compared to the difference only in December–February (DJF) (Figs. 3b,d). We form these plots with and without strong ENSO months to confirm that ENSO does not play a role. MERRA-2 data are used for the top row, whereas the bottom rows show the tropical mean QBOE or QBOW anomaly over all the datasets. The sample size varies by dataset (see Fig. 4), although the overall ratio of QBOE to QBOW months is not substantially different in DJF than in all seasons in each dataset.

Figure 3 shows that TTL QBO temperature anomalies on the equator are stronger in boreal winter than other seasons. While the QBOE minus QBOW difference in MERRA-2 has a peak at around −1.5 K in all seasons, in boreal winter this maximum difference is −2.5 K. This influence is not due to ENSO, as evident by comparing panels with and without strong ENSO months (e.g., Figs. 3c,d vs Figs. 3a,b). The tropical mean QBOE (blue) and QBOW (red) temperature anomalies are shown individually in the bottom panels across all datasets (as opposed to the QBOE minus QBOW difference). The all-season anomaly (solid curve) is calculated relative to the all-season climatology, whereas the DJF anomaly (dashed) is relative to the DJF climatology (to account for mean state changes).

Figures 3e–k demonstrate that all datasets show larger equatorial QBO temperature anomalies in boreal winter compared to the all-season mean, although the change is not significant across all datasets. Here significance was assessed at each height (and also at each latitude in Figs. 3a–d). Differences in reanalyses are largest in the tropopause region (~18 km), although there are also significant differences higher

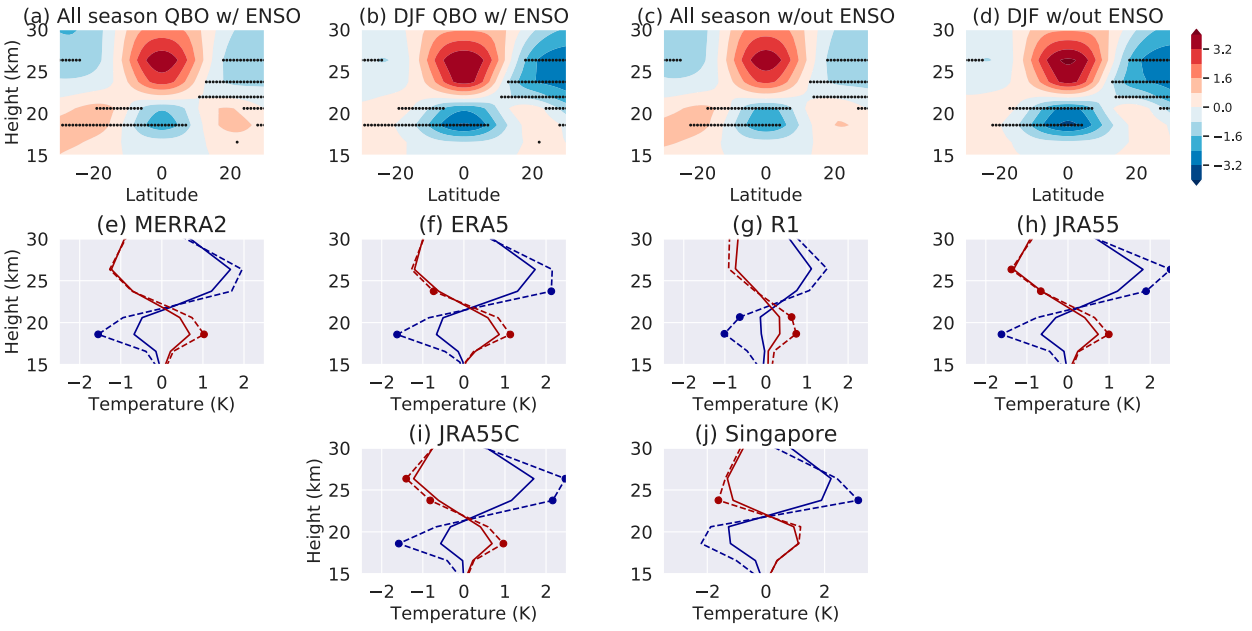

FIG. 3. MERRA-2 QBOE minus QBOW zonal-mean anomalies for (a) all months, (b) only DJF seasons, (c) all months excluding strong ENSO periods, and (d) DJF seasons excluding strong ENSO periods. (e)–(j) The QBOE (blue) and QBOW anomalies (red) in each dataset for all seasons (solid) and DJF only (dashed). Periods where the DJF difference is significantly larger than the all-seasons difference are labeled with stippling in (a)–(d) or a dot in (e)–(j).

in the stratosphere (e.g., ~26 km) with the opposite sign. All reanalysis datasets show significantly stronger QBO anomalies from 10°N to 10°S in both in the TTL around 18 km as well as at upper levels around 24 km during DJF. Both the QBOE and QBOW anomalies are stronger in DJF, in the sense that the cold QBOE anomalies are colder and the warm anomalies QBOW are warmer in winter. Also, while the all-season QBO anomalies are fairly symmetric, the DJF anomaly is stronger in

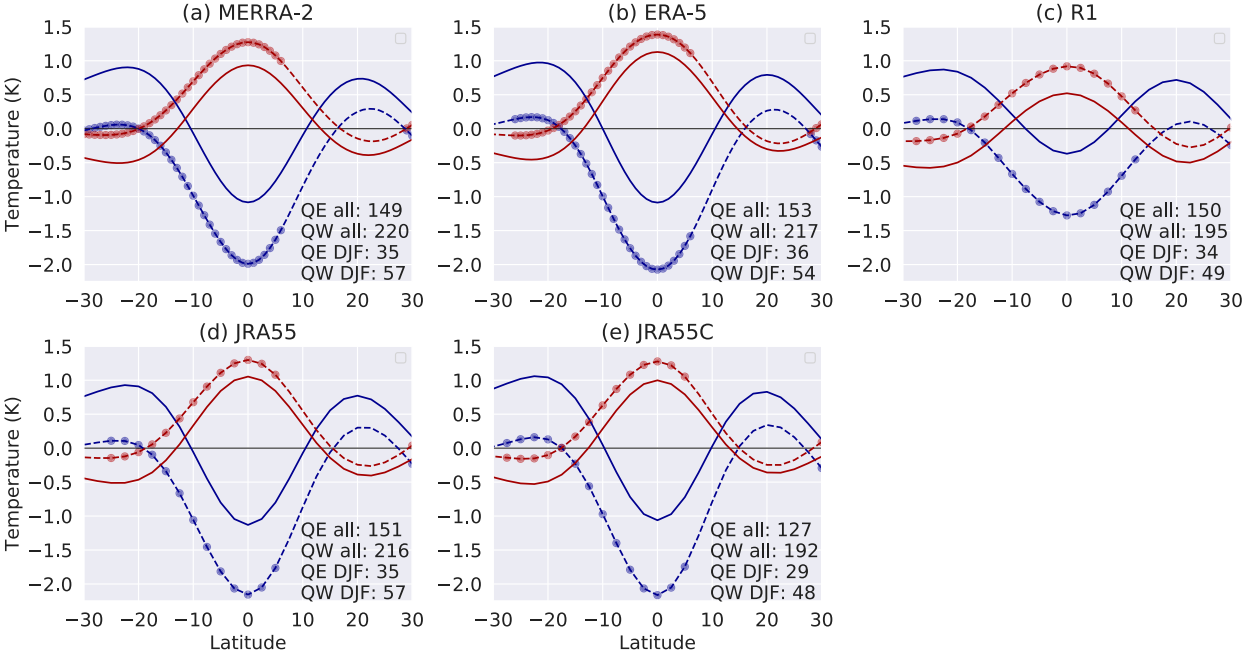

FIG. 4. Zonal-mean QBOE and QBOW temperature anomalies at 70 hPa (~18.5 km), as a function of latitude. As in Fig. 3, QBOE anomalies are in blue and QBOW anomalies are red; dashed lines are DJF and solid lines are all seasons. Points where the QBOE minus QBOW difference is significantly stronger or weaker in DJF relative to the all-season difference are marked with a dot on both DJF curves.

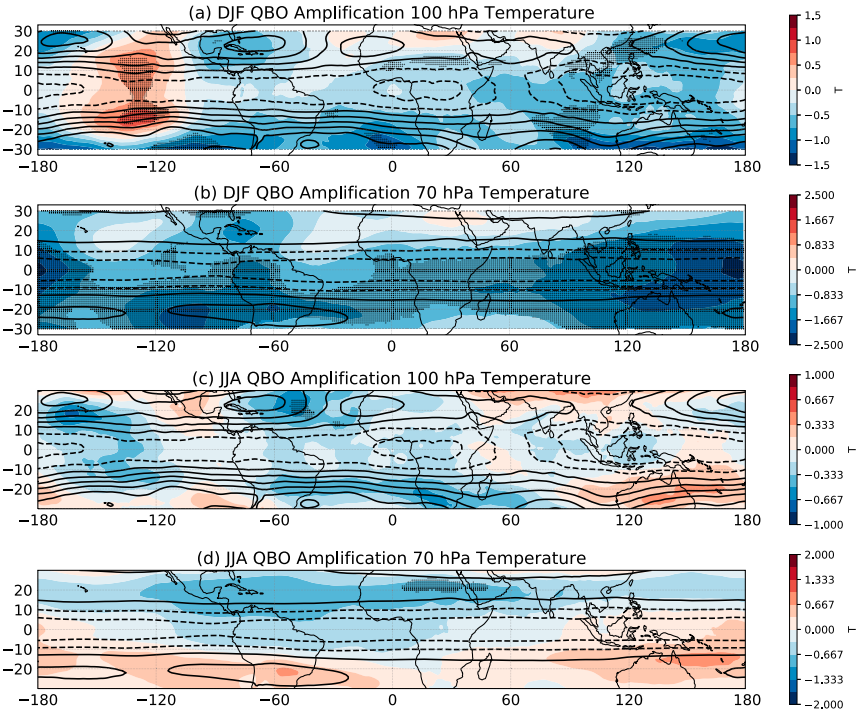

FIG. 5. The MERRA-2 QBO temperature changes at (a),(c) 100 and (b),(d) 70 hPa. Contours show the all-season QBOE minus QBOW temperature anomalies; at 100 hPa the contour interval is 0.25 K from −1.5 to 1.5 K, and at 70 hPa the interval is 1 K from −4.5 to 4.5 K (negative contours dashed). Shading shows the difference between the (a),(b) DJF or (c),(d) JJA QBOE minus QBOW differences and the all-season QBOE minus QBOW difference. Stippling indicates significant changes in DJF or JJA relative to to the all-season difference.

QBOE than in QBOW, suggesting that whatever acts to increase TTL variability associated with the QBO in DJF acts more strongly during the easterly phase than during the westerly phase.

While QBO anomalies in DJF are stronger in Singapore data than the all-season values, the differences are not significant. In this dataset, it appears the lack of significance is due to ENSO: the physical location of the Singapore sounding site is near a region where ENSO's TTL anomalies are stronger than the zonal mean, and thus ENSO has a larger effect on the sounding data than in reanalyses. Remaking Fig. 3 removing strong ENSO periods from the Singapore record leads to stronger and statistically significant DJF anomalies in Fig. 3 (not shown).

In contrast to equatorial QBO anomalies, which are stronger in DJF relative to other seasons, off-equatorial QBO anomalies are weaker in DJF than other seasons (Figs. 3a–d). In the all-season plots, warm anomalies of around 1 K are evident around 20°N/S, whereas these anomalies are essentially zero in boreal winter. This is true in all reanalysis datasets, and the structure is similar to that shown using MERRA-2. To examine this more, Fig. 4 shows the zonal-mean QBOE and QBOW temperature anomalies, as in Figs. 3e–k, taken at a fixed height of 70 hPa (~18.5 km) as a function of latitude. Dashed lines again show the DJF values, whereas solid lines show the all-season values. The on-equator strengthening is evident, and is significant across all the reanalysis products. Also evident are weaker off-equatorial anomalies in all the datasets that are statistically significant in the Southern Hemisphere and, while not significantly different, are also evident in the Northern Hemisphere subtropics.

The off-equatorial warm QBO anomalies have been attributed to a QBO meridional circulation (e.g., Baldwin et al. 2001). The equatorial cold anomaly in the TTL during QBOE is driven by adiabatic ascent whereas at upper levels the warm anomaly is driven by descent (see Fig. 11). These vertical motions form the equatorial branch of a pair of meridional overturning cells with descent in the subtropics, and that descent causes the warm anomalies in QBOE. The same argument, but with opposite signs, holds in QBOW. It is not clear why these off-equatorial anomalies should weaken despite the stronger on-equator variability, although it is clear from Fig. 4 that the overall meridional structure of the temperature fields between the DJF and all-season QBO anomalies are similar—the curves are merely shifted colder throughout the tropics and subtropics in QBOE and shifted warmer in QBOW.

The absence of a QBOE–QBOW difference in the meridional temperature structure in DJF is consistent, through thermal wind balance, with a similarly small change in the zonal wind field. Remaking Fig. 3 with zonal wind rather than temperature (not shown for all datasets, but see Fig. 11) indeed shows no change in the peak of the zonal wind anomalies

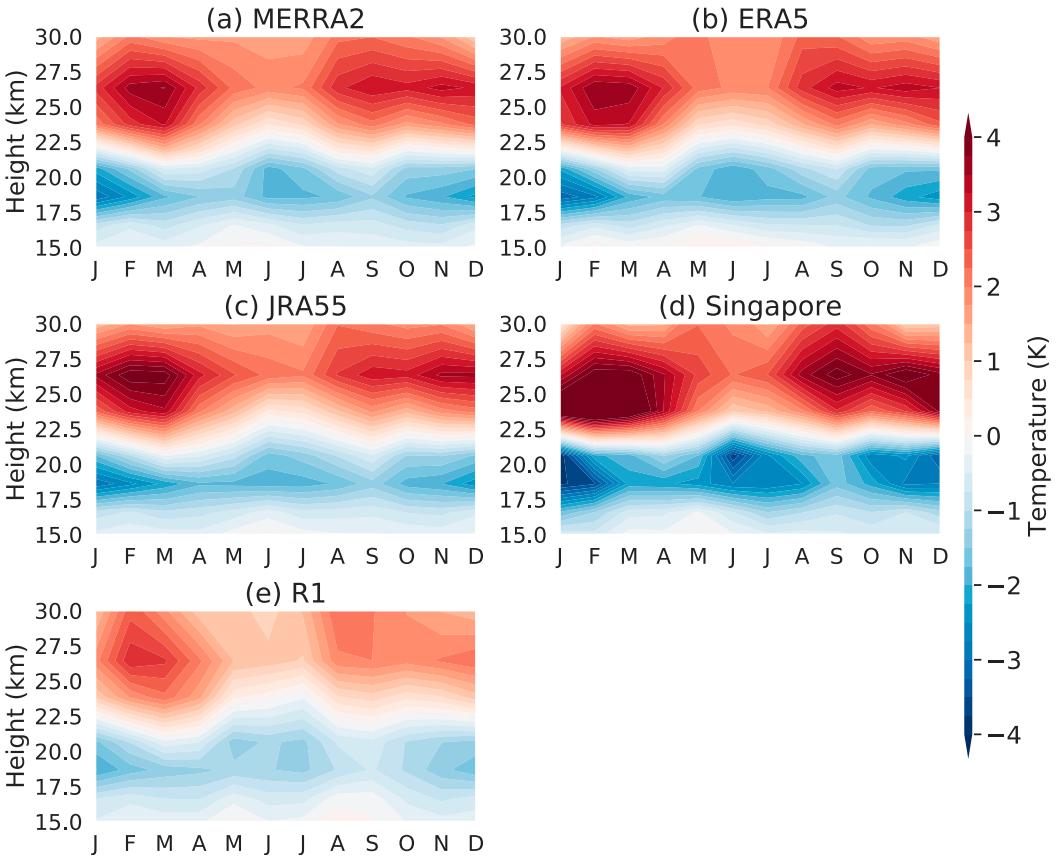

FIG. 6. Upper-tropospheric–lower-stratospheric QBOE minus QBOW temperature differences averaged over the tropics (zonally and between 10°N and 10°S) binned by month of the year (January to December on the *x* axis; height in km on *y* axis) for the (a) MERRA-2, (b) ERA5, (c) JRA-55, (d) Singapore sounding, and (e) R1 datasets. The color bar interval is 0.25 K.

between different seasons. There is a significant change in some datasets to the vertical shear of the wind at levels above around 23 km but overall signals are not as apparent in the wind as they are in temperature.

Figure 5 examines the horizonal structure of TTL QBO temperature anomalies more at 100 and 70 hPa (~16.5 and ~18.5 km, respectively) in MERRA-2. In these plots, we compare the boreal winter QBOE minus QBOW differences to the all-season difference, as well as similar plots for boreal summer. Contours in each plot show the QBOE minus QBOW climatology for all seasons. The shading is the DJF [or June–August (JJA)] QBOE minus QBOW difference subtracted from the all-season QBOE minus QBOW difference. Colder (blue) regions indicate the DJF or JJA QBO difference is colder than the all-season change, and red regions indicate the DJF or JJA QBO difference is warmer. Significance is assessed using the same bootstrapping method as above at each latitude and longitude.

In DJF a clear and strong decrease in the QBOE minus QBOW temperature difference relative to the all-season difference is evident throughout the tropics, especially at 70 hPa. This decrease in the deep tropics is consistent with stronger temperature signals, while the decrease in the subtropics is consistent with weaker QBOE minus QBOW signals. Further, the DJF enhancement is most pronounced around the Indian Ocean, the Maritime Continent, and the east Pacific at 70 hPa. Also evident at 70 hPa is significant weakening of anomalies in the Southern Hemisphere subtropics. Changes to the Northern Hemisphere subtropics, while also displaying a weaker temperature signal in DJF, are not significant, consistent with Fig. 4. At 100 hPa, changes are weaker than 70 hPa and statistical significance is more limited. Additionally, the DJF QBOE minus QBOW signal at 100 hPa is warmer in the east Pacific than the annual mean: this increase is associated with ENSO, and removing strong ENSO months removes this feature while not affecting other overall findings (not shown).

Overall, this suggests that the QBO enhancement in DJF may be particularly strong at certain longitude regions, rather than being entirely zonally symmetric. The Maritime Continent and warm pool region display some of the strongest and most persistent deep convection anywhere in the world, suggesting perhaps that some process linked to convection may be related to this enhanced temperature variability. This will be explored more in future work and is discussed briefly in section 4 in the context of the MJO; in general it remains unclear why changes are strongest in this region and what link, if any, there is between changes in QBO temperature signals and convection.

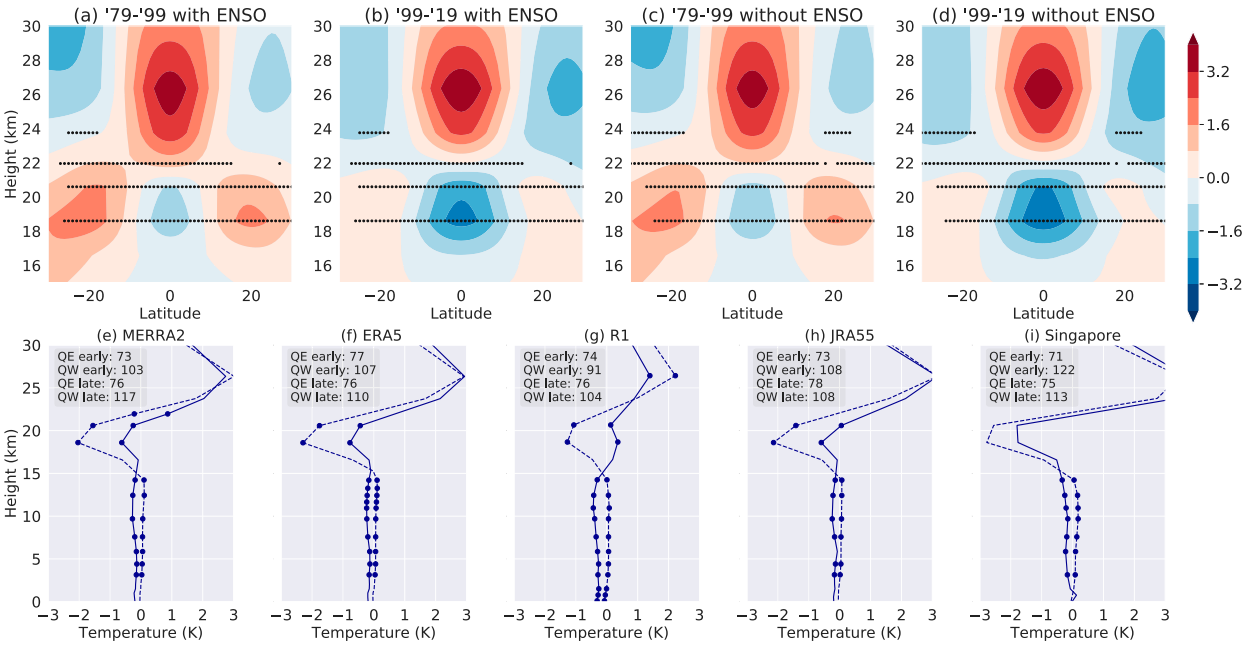

FIG. 7. Similar to Fig. 3, but showing (a),(c) the zonal-mean QBOE minus QBOW temperature anomaly in MERRA-2 from 1979–99 compared to (b),(d) the anomaly from 1999–2019 (both independent of season). Note that (a) and (b) include strong ENSO months, whereas (c) and (d) do not. (e)–(i) QBOE minus QBOW anomalies across all datasets in the early 1979–99 period (solid) vs the late 1999–2019 period (dashed). Significance is marked with stippling in (a)–(d) or a dot (e)–(i) and is calculated via the bootstrapping described in section 3c. The number of QBOE and QBOW months in the early (1979–99) and late (1999–2019) periods are listed in (e)–(i).

In addition to DJF changes, Fig. 5 also shows the JJA change in QBO temperature signals. In general, JJA signals are weaker than DJF and not significant to the same extent as DJF. QBO temperature anomalies at 70 hPa in the Northern Hemisphere subtropics around 20°N are decreased in JJA, but other regions do not show strong signals. Figure 6 further examines the seasonal cycle of QBO temperature anomalies; we plot QBOE minus QBOW temperature differences binned by month from MERRA-2, ERA5, Singapore, R1, and JRA-55. JRA-55 and JRA-55C also do not differ markedly. Figure 6 confirms the strengthening of equatorial QBO anomalies in DJF noted above, and shows a smaller local maximum around JJA, though repeating the calculations in Fig. 3 for JJA shows changes here are not significant (in agreement with Fig. 5). R1 shows weaker anomalies overall, but the same relative behavior can be seen. These plots indicate that QBO temperature anomalies undergo a semiannual cycle in amplitude. At upper levels, however (e.g., ~26 km), where the peak QBOE minus QBOW warm anomaly occurs, the phasing is somewhat different. Although there are still stronger warm anomalies around fall, late winter, and into early spring, a peak in the strength of the warm anomaly in JJA appears absent.

If TTL temperature anomalies are key to modulating the MJO, their greater amplitudes in DJF may explain why the MJO–QBO relationship is only significant in boreal winter. However, we should stress that the strongest signals observed here are at 70 hPa: stronger QBO temperature anomalies at lower levels—where it seems more plausible that temperature might affect the MJO (e.g., 100 hPa)—do not show clear signals. It therefore remains quite possible that other factors also play a role in explaining the seasonality of the MJO–QBO link, including changes to the amplitude of the MJO (which peaks in DJF), change to the meridional location of the MJO's activity (which tends to be closer to the equator in DJF), and changes to the TTL static stability at lower levels (which is lowest in DJF during QBOE; Abhik et al. 2019).

c. *QBO decadal temperature anomalies*

In this section we look at whether QBO temperature anomalies show longer-term trends or variability independent of season. We take two approaches to quantifying these longer-term changes: from the 40-yr span of data from 1979 to 2019 we first divide the record in half and separately examine the periods 1979–99 and 1999–2019. The year 1999 was chosen so that the statistics are roughly the same in each period; changing the precise year does not change the results. The numbers of QBOE and QBOW months in these two periods for each dataset are listed in Fig. 7: the number of QBOE months is nearly identical over the two periods, whereas there tend to be more QBOW months in the later period compared to the earlier period. The seasonal distribution of the QBOE and QBOW month between the 1979–99 and 1999–2019 periods is comparable (not shown). In addition to dividing the record in half, we also analyze QBOE minus QBOW temperature signals via a sliding 20-yr running window over the full period for which we have data.

Figure 7 is similar to Fig. 3, but compares the period 1979–99 to the period 1999–2019. Here we do not account for season. The bottom panels of Fig. 7 also differ from Figs. 3e–j in that we plot the QBOE minus QBOW difference, as the two phases

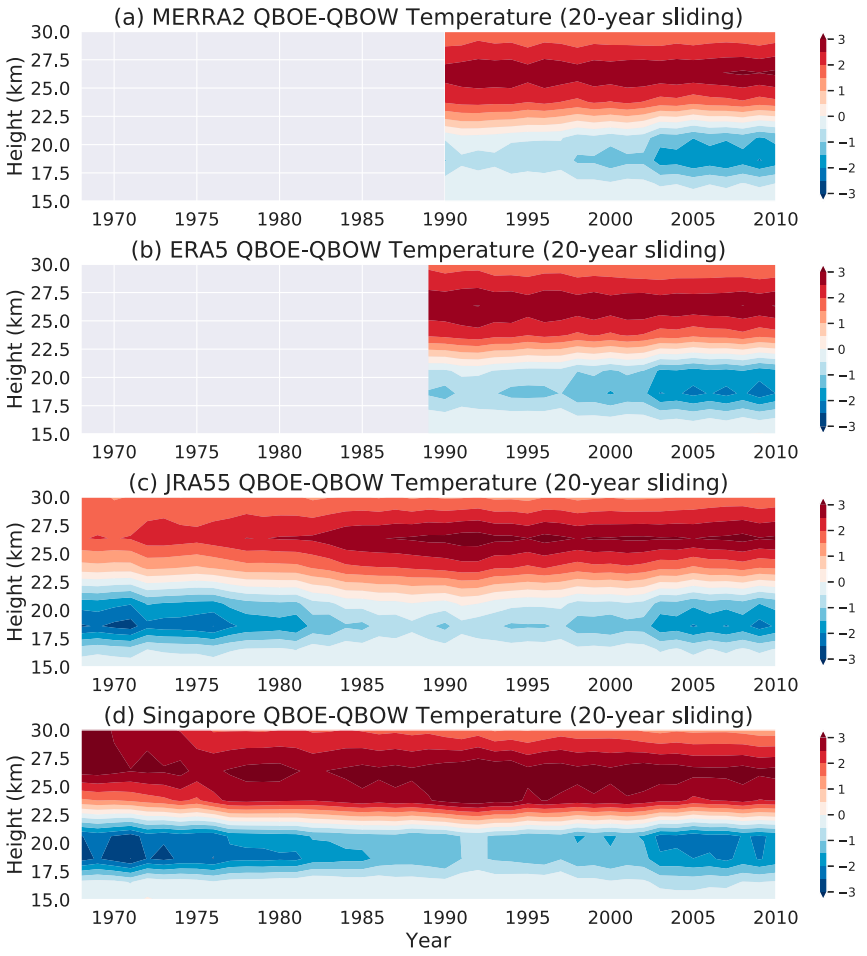

FIG. 8. QBOE minus QBOW temperature difference as a function of height averaged over the tropics. The difference is computed for a sliding 20-yr window; the *x* axis indicates the central year of the window (e.g., "1990" is the 1980–2000 QBOE minus QBOW difference). Blank spaces for MERRA-2 and ERA5 indicate a lack of data availability early in the record.

show a similar change. During these two periods, we see an enhanced equatorial QBO difference and a decreased off-equatorial QBO difference in the lower stratosphere for 1999–2019 compared to 1999–79. This is again robust across all datasets: in general, the pre-1999 QBO anomalies are on the order of −1 K, whereas the post-1999 QBO anomalies are over or around −2 K. Similar to Fig. 4, these changes in QBO temperature anomalies between decades shows the same broad shift throughout the tropics and subtropics relatively independent of latitude, with colder QBOE temperatures and warmer QBOW temperatures during the post-1999 period compared to the pre-1999 period in all reanalysis datasets. No strong changes are evident in the mid-stratosphere. For Singapore data, the difference is of the correct sign but not significant in the TTL.

In addition to the strengthening of the QBO-related TTL anomalies post-1999, another interesting feature is the small but robust difference in the troposphere between the two periods. In the early period, QBOE phases tended to be accompanied by colder tropospheric states, whereas later in the record tropospheric temperature anomalies are nearer to zero. It is possible that this signal is caused by aliasing, but restricting the dataset to only ENSO neutral years or only the DJF season, while it reduces the sample size, does not change the signal. Further, repeating our analysis after linearly detrending the data over the full period at each pressure level—to attempt to account for any sampling bias between the two periods possibly related to anthropogenic warming trends in the troposphere or cooling trends in the stratosphere—did not change our results. The stratospheric changes to the QBO temperature anomalies in Fig. 7 do not seem to be a product of changes in observing systems: the same strengthening after 1999 is evident in both JRA-55 and JRA-55C over the period where the two datasets overlap (not shown).

The JRA-55 and Singapore datasets are available from 1958, allowing us to perform analyses further back (although the amount of observed data assimilated into the reanalysis is reduced in the presatellite era). To explore temperature changes over the longer period, we calculate the QBOE minus QBOW temperature differences using a 20-yr sliding window, beginning with the period 1958–78 and ending with

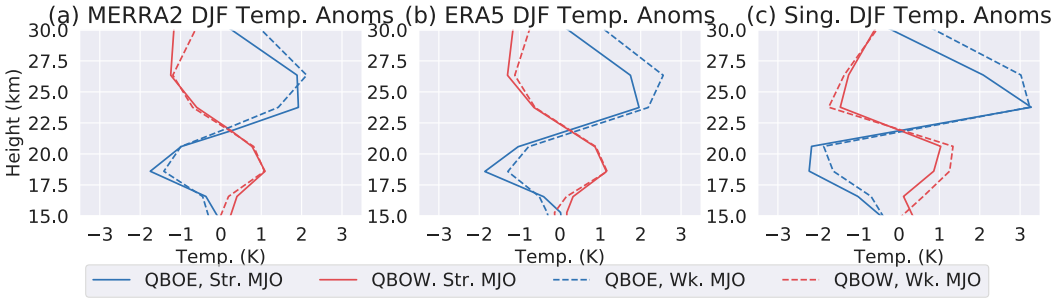

FIG. 9. (a) MERRA-2, (b) ERA5, and (c) Singapore temperature anomalies from daily data averaged zonally and from 10°N to 10°S. Blue curves are anomalies composited over QBOE periods in DJF relative to the DJF mean. Red curves are similarly DJF anomalies during QBOW periods. The solid vs dashed lines are composites from days in DJF and the specified QBO phase on which the MJO was strong (solid) or weak (dashed).

the period 1998–2018. Each 20-yr period yields one vertical profile of the QBOE minus QBOW temperature difference, and sliding the window allows us to plot how that profile changes smoothly in time. The results are shown in Fig. 8; the top two panels are for MERRA-2 and ERA5 (which have a shorter data records) and bottom panels show JRA-55 and Singapore.

The MERRA-2 and ERA5 data confirm the previous results showing a strengthening of QBO temperature differences in the lower stratosphere during last several decades. Similar signals from 1979 to 2018 are evident in JRA-55 and Singapore. However, we additionally see strong equatorial QBO temperature differences in the earliest part of the record from approximately 1958 to 1978 in JRA-55 and Singapore data. This suggests that the stronger QBO anomalies in recent decades may be oscillatory in nature rather than due to a trend. That JRA-55 and Singapore show similar behavior adds confidence to the results (although JRA-55 likely assimilates Singapore sounding data, meaning that the two datasets are not entirely independent).

Our finding here is somewhat distinct from analysis by Klotzbach et al. (2019), who looked at whether QBO temperature anomalies change on decadal time scales. There, they found via a linear trend analysis that both QBOE and QBOW 100-hPa temperatures and static stability around this level showed similar trends, such that there was no change in the QBOE minus QBOW difference during the period from 1960–2015. The difference here is that we consider the temperatures at higher levels than 100 hPa, and also do not restrict our analysis to the warm pool region. We find that changes are indeed small at 100 hPa and below (not shown), while being very clear at 70 hPa.

While QBO changes are more striking at these high levels, it is also not clear what influence if any QBO temperature signals this high up may have on the MJO. For example, we conducted an analysis of the correlation between the MJO and QBO similar to Klotzbach et al. (2019) over the periods 1979–99 and 1999–2019 (not shown) and found no strong differences between the MJO–QBO link. Our finding that QBO temperature anomalies were strong in the two decades prior to 1979 (Fig. 8) also seems inconsistent with the weak MJO–QBO link during that period (e.g., Klotzbach et al. 2019). It may, however, help explain why Klotzbach et al. (2019) saw no trend in QBOE and QBOW TTL temperatures when considering the 1960–2015 period, since the changes we find are not monotonic over that period. Thus, similar to section 3b, it remains unclear whether and how our findings in this section may relate the MJO–QBO relationship.

Irrespective of their link to the MJO, changes in the QBO structure between decades, as well as in boreal winter, are of interest in their own right. The causes of these differences are not known, but the next section shows some evidence for or against different mechanisms and offers suggestions for future work.

4. Possible mechanisms

At present it is not clear to us what causes the observed differences in QBO temperature signals, either seasonally or

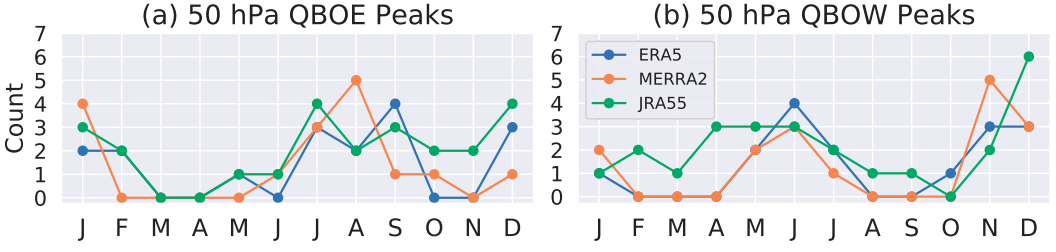

FIG. 10. A histogram of the number of (a) QBOE and (b) QBOW peaks at 50 hPa in each month, with peaks identified per section 2. Datasets are ERA5, MERRA-2, and JRA-55. The *x* axis is months, as in Fig. 6. Note for JRA-55 the full span of available dates beginning in 1958 was used.

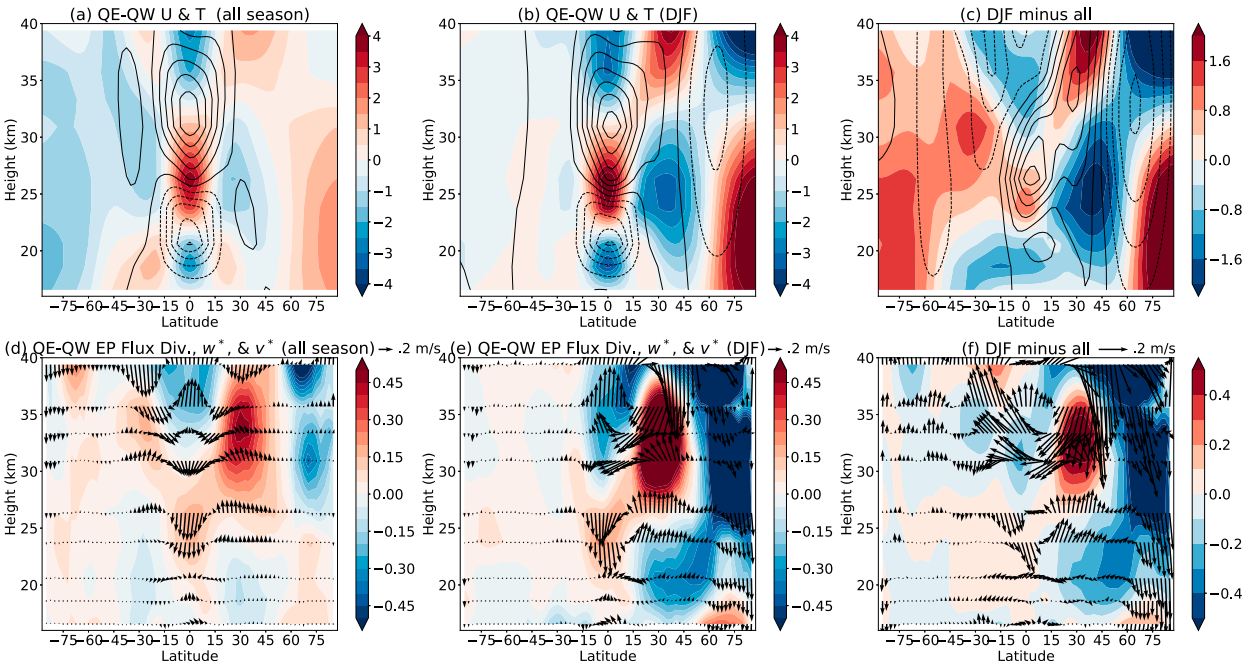

FIG. 11. ERA-Interim QBOE minus QBOW difference plots of (a)–(c) zonal-mean wind anomalies (contours; m s^{-1}) and temperature (shading; K) and (d)–(f) EP flux divergence (shading; kg s^{-1} day^{-1}), and residual circulation anomalies (v*, w*; arrows). For visualization, w* has been multiplied by 1000 (units are mm s^{-1}; for v* units are m s^{-1}): the arrow scale is given in the title. Columns show (a),(d) the QBO differences using all months, (b),(e) the difference restricted to DJF, and (c),(f) the DJF difference minus the all-month difference. In (a) and (b) wind contours are from −30 to 30 m s^{-1} at 5 m s^{-1} intervals and in (c) contours are from −10 to 10 m s^{-1} at 2 m s^{-1} intervals, with negative contours dashed.

on longer time scales. Three hypotheses we explore are 1) whether the MJO plays an active role in generating the observed QBO temperature differences in the TTL, 2) whether differences are a by-product of phase locking between the QBO and the annual cycle, and 3) whether changes to the large-scale stratospheric circulation may play a role. None seems to explain the observed changes to QBO temperatures fully.

a. MJO impact and QBO transition timing

To examine whether the MJO plays an active role in generating the QBO TTL signals described in the preceding sections, Fig. 9 shows composites using daily data to look at periods when the MJO is strong or weak, controlling for the phase of the QBO and the season to avoid aliasing. We use daily data from Singapore, ERA5, and MERRA-2. Figure 9 plots the anomalous TTL temperatures in DJF (relative to the DJF climatology) during QBOE and QBOW periods in blue and red, respectively. We further segregate the data based on days when the MJO is strong (solid) and days when the MJO is weak (dashed).

Whether the MJO is strong or weak does not appear to explain the enhancement in QBO temperatures in DJF. QBOW temperature anomalies in Fig. 9 are the same regardless of the strength of the MJO, such that stronger MJO events in DJF are likely not the cause of the enhanced anomalies. There is also not much change in QBOE: the TTL anomaly is slightly colder when the MJO is strong than when it is weak, but the change is smaller than the differences in DJF discussed in section 3b. Remaking these composites with monthly data shows stronger MJO signals, in particular indicating stronger cold anomalies in QBOE when the MJO is strong versus weak (not shown). However, due to the restrictive compositing by season, QBO phase, and MJO strength, the number of data points using monthly data is very limited and hampers statistical significance and meaningful interpretation. Further analysis looking at correlations between MJO strength and the strength of QBO temperature anomalies did not reveal any strong link between the two (not shown). We also examined whether there is an overall trend in MJO strength from 1979–2018 and were unable to demonstrate any strengthening of the MJO during this period which may explain decadal changes. It therefore seems unlikely that changes to the MJO cause differences in QBO TTL temperature signals.

Another hypothesis for why the QBO demonstrates stronger temperature anomalies in DJF relative to other time periods is that it is a by-product of phase-locking between the QBO and the annual cycle. This phase-locking has been previously discussed in the literature [see a review in Baldwin et al. (2001) and more recently Rajendran et al. (2016)]: the QBO tends to preferentially undergo transitions in phase (at 50 hPa) in the boreal spring. We can similarly assess in which months the approximate peak of the QBO occurs. We identify peaks in the data by looking for months containing local extrema via the

methodology described in section 2. Once the peaks were identified, a histogram of the month during which they occurred was constructed for QBOE and QBOW. Results from ERA5, MERRA-2, and JRA-55 are shown in Fig. 10. Note for JRA-55, all data were included from 1958 onward to maximize the number of samples. Figure 10 shows a bimodal distribution of peaks centered roughly in the winter and summer seasons in both QBOE and QBOW at 50 hPa, consistent with the bimodal distribution of the temperature peaks in the lower stratosphere (e.g., the bottom portion of Fig. 6). However, the more fundamental question of why the QBO sometimes phase locks to the annual cycle is not established. And examination of whether this phase locking may have changed on decadal time scales and could contribute to the signals noted in section 3c yielded no conclusive results.

b. *Changes to the large-scale stratospheric circulation*

Given the fact that the shifts in the QBOE and QBOW temperature anomalies are approximately independent of latitude within a wide band encompassing the tropics and subtropics (e.g., Fig. 4), another plausible hypothesis is that the Brewer–Dobson circulation (Butchart 2014) and associated large-scale upwelling in the TTL and lower stratosphere may interact more strongly with the QBO in the solstice seasons (especially DJF). Because the anomalous upwelling or downwelling associated with the BDC tends to be broad throughout the tropics, changes to this upwelling might explain why the temperature anomalies are shifted more negative in QBOE and more positive in QBOW in a relatively uniform manner between ~30°S and 30°N.

A connection between the QBO and the stratospheric large-scale circulation, including the BDC, has been studied most extensively in the context of the QBO impact on the stratospheric polar vortex, particularly in the Northern Hemisphere. Both modeling (e.g., O'Sullivan and Young 1992; Kinnersley and Tung 1999; Naito and Yoden 2006; Pascoe et al. 2006; Hampson and Haynes 2006) and observational studies (e.g., Dunkerton and Baldwin 1991; Garfinkel and Hartmann 2007; Hitchman and Huesmann 2009) have demonstrated that the QBO can alter the strength of the vortex, with warmer polar cap temperatures and a weaker, more frequently disrupted vortex during QBOE compared to QBOW. The mechanism by which the QBO impacts the polar vortex is still not entirely well understood, but is thought to involve QBO-induced changes to wave propagation, via the so-called Holton–Tan effect (Holton and Tan 1980). Studies have proposed that these changes are due to QBO winds altering the location of the zero-wind line (Holton and Tan 1980), or might be attributed to changes in the QBO meridional circulation (Garfinkel et al. 2012; Watson and Gray 2014; White et al. 2015).

The focus of many of these studies has been on the QBO impacts in the midlatitudes and polar regions. The response within the tropics and around the TTL has been less considered. Those works that examine the links between the QBO, the BDC and tropical upwelling (e.g., Niwano et al. 2003; Fujiwara et al. 2010; Flury et al. 2013; Neu et al. 2014; Rao et al. 2019), have generally found a stronger BDC in QBOE and a weaker BDC in QBOW, although mechanisms connecting the QBO and the BDC in the tropics are not clear (Flury et al. 2013; Neu et al. 2014), and the seasonality of any connection has not been explored.

As a preliminary analysis, we examined QBOE minus QBOW changes in the zonal-mean stratospheric residual circulation and EP flux divergence in all seasons compared to the same difference in DJF. Figure 11 shows the QBOE minus QBOW change in the zonal wind (Figs. 11a–c; contours), temperature (Figs. 11a–c; shading), EP flux divergence (Figs. 11d–f; shading), and residual circulation (Figs. 11d–f; arrows) throughout the global stratosphere. The rightmost panel shows the DJF minus all-season change (e.g., the central panels minus left panels).

Many of the features already discussed regarding changes to QBO temperature signals in DJF are evident in Fig. 11. In particular, the key features we have addressed are evident in the lower-stratospheric tropics and subtropics: at ~20 km the stronger equatorial cold anomalies and weaker subtropical warm anomalies in DJF are evident. In Fig. 11c, we clearly see the DJF temperature change in QBOE minus QBOW is stronger (e.g., more negative) over a broad swath of the deep and subtropical TTL. In addition to the changes in the TTL, stronger QBO temperature changes during DJF are also evident in the upper-stratospheric tropics, Northern Hemisphere midlatitudes, and the poles. We discuss these differences briefly before returning to the tropical TTL.

In the Northern Hemisphere polar region, the QBOE minus QBOW temperature change (a warmer polar cap throughout much of the stratosphere poleward of 60°N) is consistent with the warming associated with the Holton–Tan effect and a QBO impact on the vortex, as noted for example in Holton and Tan (1980), Garfinkel et al. (2012), and White et al. (2015). This anomalous warming is accompanied by anomalous downwelling evident in the residual circulation (Figs. 11d–f) in QBOE relative to QBOW.

Outside of the polar region and above ~23 km, QBO temperature changes in the midlatitudes and tropics during DJF appear consistent with strengthened QBO meridional overturning circulation in boreal winter. For example, the warm anomaly centered at ~25 km on the equator is warmer in DJF, and the cold anomaly at the same level centered around 30°N is colder in DJF than the all-season average. The same pattern, with the opposite sign, is evident at the highest levels near ~35 km. Studies have noted that the QBO meridional circulation tends to strengthen and favor the winter hemisphere during solstice seasons (Jones et al. 1998; Kinnersley and Tung 1998, 1999; Kinnersley 1999; Peña-Ortiz et al. 2008), and indeed the residual circulation anomalies in Fig. 11 support the interpretation that stronger temperature signals here are due to stronger adiabatic warming or cooling driven by the circulation, while the summer hemisphere shows weaker temperature and circulation signals.

However, note this does not appear to be the case in the TTL, where no strong off-equatorial temperature anomaly is observed in either hemisphere. Thus, while seasonal QBO temperature amplitudes at upper levels seem related to seasonal changes in the QBO meridional circulation, QBO changes in the TTL appear to be modulated by a separate process. A similar analysis comparing the all-season change to JJA (not shown) showed different behavior in this season: there the warm anomaly in the Southern Hemisphere subtropics

was slightly stronger, and the warm anomaly in the Northern Hemisphere was weaker, consistent with a change in the QBO meridional circulation in the TTL. This supports the hypothesis that the observed changes in the DJF QBO temperature signals are not due to changes in the QBO meridional circulation at low levels, and that the process at play is perhaps unique to the winter solstice season.

Analysis of the zonal wind and EP flux divergence changes is also hard to connect to any differences observed in tropical TTL temperatures. The contours in Figs. 11a–c show changes to the QBO zonal winds. As noted above, little change in the wind signals is evident in the tropical lower stratosphere where the QBO winds are easterly. This lack of a strong change in the zonal wind is theoretically consistent with the lack of change in the meridional temperature gradients observed in DJF. However, at upper levels (e.g., above ~25 km), stronger anomalous QBO westerlies are observed in DJF on the equator and into the midlatitudes, while easterly anomalies are evident at the poles. The easterly anomalies, consistent with a weaker polar vortex, demonstrate the enhanced Holton–Tan effect in winter.

Figures 11d–f shows the EP-flux divergence differences in all seasons versus DJF. The sign convention here is such that negative (blue) anomalies are associated with less divergence (e.g., anomalous convergence) and positive anomalies indicate increased divergence. Overall, the EP flux divergence changes in QBOE versus QBOW during DJF are consistent with the patterns observed by other studies [see, e.g., schematics in Garfinkel et al. (2012) and White et al. (2015)]. The overall pattern of the EP flux divergence is similar in DJF compared to the all-season pattern in the Northern Hemisphere, except that the pattern is much stronger in DJF. This is consistent with a stronger effect of waves on the stratospheric dynamics in this season, as westerly flow allows more waves to propagate into the boreal winter stratosphere. In the lower stratosphere tropics and subtropics, QBO easterlies inhibit planetary wave propagation into the tropics, leading to an increased EP flux convergence throughout much of the lower-stratospheric midlatitudes (the blue anomaly from 15° to 60°N below ~25 km). The wave forcing at upper levels in the midlatitudes is the opposite sign, with an increased divergence in the midlatitudes in DJF driving stronger EP flux convergence in the tropics and at the poles above ~30 km. This divergence likely helps drive the enhanced QBO residual circulation at upper levels, which may contribute the stronger warm anomalies in the tropics centered around 25 km and the increased westerlies there.

Overall, however, both the zonal wind and EP flux divergence do not show strong changes in the tropical TTL in DJF compared to all seasons, despite the change in the temperature anomalies there. Further, upwelling associated with the residual circulation (w^*) does not appear to entirely explain the DJF enhancement of temperatures, as one might expect if the temperature enhancement in DJF were due to an overall change in the deep branch of the BDC. At 70 hPa (~18.5 km) it is difficult to detect a clear increase across the tropics and subtropics in upwelling associated with the residual circulation in Fig. 11. A more detailed analysis compositing the QBOE minus QBOW changes in w^* at 100 and 70 hPa (not shown) did not yield any more conclusive results. We further calculated the total vertical mass flux associated with the upwelling branch of the BDC in QBOE versus QBOW to examine whether clear changes were observed in DJF. This was calculated by integrating w^* weighted by the density of air (denoted ρ) and cosine of latitude over the region in the tropics where w^* is upward. Explicitly, for each month of data we first found the latitudes, ϕ_1 and ϕ_2, where w^* changed sign from upward (in the tropics) to downward (in the midlatitudes); requiring that $|\phi_{1,2}| \geq 10$ to ensure the broad tropical upwelling signals was captured. We then calculated the upward mass flux M_{up}:

$$M_{\text{up}} = 2\pi a^2 \int_{\phi_1}^{\phi_2} \rho(\phi) w^*(\phi) \cos(\phi)\, d\phi,$$

where a is the radius of Earth. We found the all-season mean upward mass flux at 70 hPa to be approximately $7.10 \times 10^9\,\text{kg s}^{-1}$, comparable to estimates reported in other studies (e.g., Lin and Fu 2013; Rao et al. 2019). The all-season QBOE minus QBOW change in M_{up} was $0.80 \times 10^8\,\text{kg s}^{-1}$, as compared to the DJF QBOE minus QBOW change which of $2.51 \times 10^8\,\text{kg s}^{-1}$. The sign in both instances qualitatively consistent with a stronger upwelling in QBOE versus QBOW, as proposed in other studies (e.g., Flury et al. 2013), and the upwelling is more than 3 times stronger in DJF, consistent with the hypothesis that the deep branch of the BDC is stronger and modulates the QBO more in winter. However, a bootstrap analysis found that this enhancement in the upward mass flux at 70 hPa in DJF was not statistically significant. Thus, it is difficult to conclude that the changes to QBO temperature anomalies are due to changes in tropical upwelling. Conducting a similar analysis during the early and late periods to look at whether these processes might explain decadal changes in the QBO similarly did not yield results in the TTL that seemed to explain observed temperature changes.

5. Conclusions

This study examines TTL temperature anomalies, focusing especially on those associated with the QBO. We are motivated by the strong link between the QBO and the MJO, in which TTL temperature anomalies have been hypothesized to play a key role. In particular, we examined whether the seasonality of the MJO–QBO link (it is only significant in boreal winter; Yoo and Son 2016) and its emergence only in recent decades (Klotzbach et al. 2019) can be linked to changes in QBO temperature anomalies during these periods. We hypothesize that stronger QBO temperature anomalies could help explain the stronger MJO–QBO connection. We find that QBO temperature anomalies in the TTL are indeed modulated on both annual and decadal time scales, although the link to the MJO–QBO connection remains unclear. Our main results can be summarized as follows:

1) On annual time scales, QBO temperature anomalies on the equator are stronger (i.e., colder in QBOE and warmer in QBOW) in boreal winter than during the rest of the year (Fig. 3). Off-equatorial QBO temperature anomalies, on the other hand, are weaker in boreal winter than in the all-season mean (Figs. 3–5), with large differences in particular

around the Maritime Continent and the west Pacific (Fig. 5). Thus, the strength of both the equatorial and off-equatorial QBO temperature anomalies is distinctly different in DJF than in other seasons. The difference can be viewed as a shift in DJF QBO temperature anomalies that is relatively independent of latitude within a broad range encompassing the subtropics. Thus, the meridional structure and (by thermal wind balance) the associated zonal wind anomalies do not show strong differences in DJF compared to the all-season mean.

2) The same on-equatorial strengthening and off-equatorial weakening of QBO temperature anomalies occurs on decadal time scales. The period 1999–2019 showed stronger equatorial QBO anomalies than the period 1979–99 (Fig. 7). In one reanalysis dataset that extends back to 1958 (JRA-55), as well as in the Singapore sounding data, we further found that 1958–78 also had stronger equatorial QBO temperature anomalies relative to 1978–98 (Fig. 8).

We are unable to explain the cause of these changes to QBO temperature anomalies. It appears unlikely that an upward influence due to the MJO causes these changes (Fig. 9). We find, consistent with previous literature (e.g., Rajendran et al. 2016), that the QBO winds at 50 hPa tend to phase-lock to the annual cycle and peak in the solstice seasons (Fig. 10), when temperature anomalies are strongest. But this argument cannot be causally disentangled without a mechanism explaining why either the temperature or the wind should synchronize with the annual cycle. A preliminary analysis of the residual circulation (Fig. 11) shows distinct circulation and temperature patterns globally in QBOE minus QBOW in boreal winter compared to the all-season changes. Temperature and circulation changes are particularly clear in the midlatitudes and polar regions (which we attribute to the Holton–Tan effect), but changes in the residual circulation in the tropics are more subtle. At upper levels, QBO temperature changes seem due to a stronger QBO meridional circulation, as noted in other studies (e.g., Jones et al. 1998; Kinnersley and Tung 1998, 1999; Peña-Ortiz et al. 2008), but in the TTL this does not appear to be the case. We found no clear upwelling or circulation changes that seemed to explain the changes we observe in temperature anomalies in the TTL. However, our analysis of the residual circulation is preliminary and future work exploring this more should be carried out, in particular since the representation of the BDC in reanalysis can vary substantially (e.g., Abalos et al. 2015). It is further possible that processes we have not explored or discussed, such as ozone or cloud feedbacks, might have a role in modulating QBO temperature anomalies across these time scales. In particular, if dynamical processes cannot explain these changes, it seems like that radiative changes, perhaps linked to changes in ozone or water vapor, may play a role.

Acknowledgments. This work was supported by NSF AGS-1543932 and by NASA Headquarters under the NASA Earth and Space Science Fellowship Program (Grant 80NSSC18K1347). Thanks to George Kiladis, Ed Gerber, and Matthew Hitchman for helpful and encouraging conversations and guidance on this work at various stages.

Data availability statement. All datasets used in this study are publicly available. The RMM index is available at http://www.bom.gov.au/climate/mjo/graphics/rmm.74toRealtime.txt. The Niño-3.4 index is available at https://www.esrl.noaa.gov/psd/gcos_wgsp/Timeseries/Data/nino34.long.anom.data. Reanalysis datasets are all publicly available at locations cited in the appropriate references. The Singapore sounding data retrieved through the Integrated Global Radiosonde Archive are available at https://www1.ncdc.noaa.gov/pub/data/igra/. The zonal-mean diagnostics calculations are available publicly (see Martineau 2017; https://doi.org/10.5285/b241a7f536a244749662360bd7839312) and are archived and maintained by the Centre for Environmental Data Analysis (CEDA: https://catalogue.ceda.ac.uk/uuid/b241a7f536a244749662360bd7839312).

REFERENCES

Abalos, M., B. Legras, F. Ploeger, and W. J. Randel, 2015: Evaluating the advective Brewer–Dobson circulation in three reanalyses for the period 1979–2012. *J. Geophys. Res. Atmos.*, **120**, 7534–7554, https://doi.org/10.1002/2015JD023182.

Abhik, S., H. H. Hendon, and M. C. Wheeler, 2019: On the sensitivity of convectively coupled equatorial waves to the quasi-biennial oscillation. *J. Climate*, **32**, 5833–5847, https://doi.org/10.1175/JCLI-D-19-0010.1.

Andrews, D. G., J. R. Holton, and C. B. Leovy, 1987: *Middle Atmosphere Dynamics*. Academic Press, 489 pp.

Baldwin, M. P., and Coauthors, 2001: The quasi-biennial oscillation. *Rev. Geophys.*, **39**, 179–229, https://doi.org/10.1029/1999RG000073.

Butchart, N., 2014: The Brewer–Dobson circulation. *Rev. Geophys.*, **52**, 157–184, https://doi.org/10.1002/2013RG000448.

Dee, D. P., and Coauthors, 2011: The ERA-Interim reanalysis: Configuration and performance of the data assimilation system. *Quart. J. Roy. Meteor. Soc.*, **137**, 553–597, https://doi.org/10.1002/qj.828.

Domeisen, D. I., C. I. Garfinkel, and A. H. Butler, 2019: The teleconnection of El Niño Southern Oscillation to the stratosphere. *Rev. Geophys.*, **57**, 5–47, https://doi.org/10.1029/2018RG000596.

Dunkerton, T. J., and M. P. Baldwin, 1991: Quasi-biennial modulation of planetary wave fluxes in the Northern Hemisphere winter. *J. Atmos. Sci.*, **48**, 1043–1061, https://doi.org/10.1175/1520-0469(1991)048<1043:QBMOPW>2.0.CO;2.

Durre, I., and X. Yin, 2008: Enhanced radiosonde data for studies of vertical structure. *Bull. Amer. Meteor. Soc.*, **89**, 1257–1262, https://doi.org/10.1175/2008BAMS2603.1.

——, R. S. Vose, and D. B. Wuertz, 2006: Overview of the Integrated Global Radiosonde Archive. *J. Climate*, **19**, 53–68, https://doi.org/10.1175/JCLI3594.1.

Flury, T., D. L. Wu, and W. G. Read, 2013: Variability in the speed of the Brewer–Dobson circulation as observed by Aura/MLS. *Atmos. Chem. Phys.*, **13**, 4563–4575, https://doi.org/10.5194/acp-13-4563-2013.

Fueglistaler, S., A. E. Dessler, T. J. Dunkerton, I. Folkins, Q. Fu, and P. W. Mote, 2009: Tropical tropopause layer. *Rev. Geophys.*, **47**, RG1004, https://doi.org/10.1029/2008RG000267.

Fujiwara, M., and Coauthors, 2010: Seasonal to decadal variations of water vapor in the tropical lower stratosphere observed with balloon-borne cryogenic frost point hygrometers. *J. Geophys. Res.*, **115**, D18304, https://doi.org/10.1029/2010JD014179.

——, and Coauthors, 2017: Introduction to the SPARC Reanalysis Intercomparison Project (S-RIP) and overview of the reanalysis systems. *Atmos. Chem. Phys.*, **17**, 1417–1452, https://doi.org/10.5194/acp-17-1417-2017.

Garfinkel, C. I., and D. L. Hartmann, 2007: Effects of the El Niño–Southern Oscillation and the quasi-biennial oscillation on polar temperatures in the stratosphere. *J. Geophys. Res.*, **112**, D19112, https://doi.org/10.1029/2007JD008481.

——, T. A. Shaw, D. L. Hartmann, and D. W. Waugh, 2012: Does the Holton–Tan mechanism explain how the quasi-biennial oscillation modulates the Arctic polar vortex? *J. Atmos. Sci.*, **69**, 1713–1733, https://doi.org/10.1175/JAS-D-11-0209.1.

Gelaro, R., and Coauthors, 2017: The Modern-Era Retrospective Analysis for Research and Applications, version 2 (MERRA-2). *J. Climate*, **30**, 5419–5454, https://doi.org/10.1175/JCLI-D-16-0758.1.

Gettelman, A., and P. M. de Forster, 2002: A climatology of the tropical tropopause layer. *J. Meteor. Soc. Japan*, **80**, 911–924, https://doi.org/10.2151/jmsj.80.911.

Hampson, J., and P. Haynes, 2006: Influence of the equatorial QBO on the extratropical stratosphere. *J. Atmos. Sci.*, **63**, 936–951, https://doi.org/10.1175/JAS3657.1.

Hendon, H. H., and S. Abhik, 2018: Differences in vertical structure of the Madden–Julian oscillation associated with the quasi-biennial oscillation. *Geophys. Res. Lett.*, **45**, 4419–4428, https://doi.org/10.1029/2018GL077207.

Hersbach, H., and Coauthors, 2019: Global reanalysis: Goodbye ERA-Interim, hello ERA5. *ECMWF Newsletter*, No. 159, ECMWF, Reading, United Kingdom, 17–24, http://ecmwf.int/sites/default/files/elibrary/2019/19027-global-reanalysis-good-bye-era-interim-hello-era5.pdf.

Hitchman, M. H., and A. S. Huesmann, 2009: Seasonal influence of the quasi-biennial oscillation on stratospheric jets and Rossby wave breaking. *J. Atmos. Sci.*, **66**, 935–946, https://doi.org/10.1175/2008JAS2631.1.

Holton, J. R., and H. C. Tan, 1980: The influence of the equatorial quasi-biennial oscillation on the global circulation at 50 mb. *J. Atmos. Sci.*, **37**, 2200–2208, https://doi.org/10.1175/1520-0469(1980)037<2200:TIOTEQ>2.0.CO;2.

Huesmann, A. S., and M. H. Hitchman, 2001: The stratospheric quasi-biennial oscillation in the NCEP reanalyses: Climatological structures. *J. Geophys. Res.*, **106**, 11 859–11 874, https://doi.org/10.1029/2001JD900031.

Jones, D. B. A., H. R. Schneider, and M. B. McElroy, 1998: Effects of the quasi-biennial oscillation on the zonally averaged transport of tracers. *J. Geophys. Res.*, **103**, 11 235–11 249, https://doi.org/10.1029/98JD00682.

Jucker, M., and E. P. Gerber, 2017: Untangling the annual cycle of the tropical tropopause layer with an idealized moist model. *J. Climate*, **30**, 7339–7358, https://doi.org/10.1175/JCLI-D-17-0127.1.

Kalnay, E., and Coauthors, 1996: The NCEP/NCAR 40-Year Reanalysis Project. *Bull. Amer. Meteor. Soc.*, **77**, 437–472, https://doi.org/10.1175/1520-0477(1996)077<0437:TNYRP>2.0.CO;2.

Kim, H., J. H. Richter, and Z. Martin, 2019: Insignificant QBO–MJO prediction skill relationship in the SubX and S2S subseasonal reforecasts. *J. Geophys. Res. Atmos.*, **124**, 12 655–12 666, https://doi.org/10.1029/2019JD031416.

Kim, Hera, S.-W. Son, and C. Yoo, 2020: QBO modulation of the MJO-related precipitation in East Asia. *J. Geophys. Res. Atmos.*, **125**, e2019JD031929. https://doi.org/10.1029/2019JD031929.

Kim, Hyemi, J. Caron, J. Richter, and I. Simpson, 2020: The lack of QBO–MJO connection in CMIP6 models. *Geophys. Res. Lett.*, **47**, e2020GL087295, https://doi.org/10.1029/2020GL087295.

Kinnersley, J. S., 1999: Seasonal asymmetry of the low- and middle-latitude QBO circulation anomaly. *J. Atmos. Sci.*, **56**, 1140–1153, https://doi.org/10.1175/1520-0469(1999)056<1140:SAOTLA>2.0.CO;2.

——, and K. K. Tung, 1998: Modeling the global interannual variability of ozone due to the equatorial QBO and to extratropical planetary wave variability. *J. Atmos. Sci.*, **55**, 1417–1428, https://doi.org/10.1175/1520-0469(1998)055<1417:MTGIVO>2.0.CO;2.

——, and ——, 1999: Mechanisms for the extratropical QBO in circulation and ozone. *J. Atmos. Sci.*, **56**, 1942–1962, https://doi.org/10.1175/1520-0469(1999)056<1942:MFTEQI>2.0.CO;2.

Kistler, R., and Coauthors, 2001: The NCEP–NCAR 50-Year Reanalysis: Monthly means CD-ROM and documentation. *Bull. Amer. Meteor. Soc.*, **82**, 247–268, https://doi.org/10.1175/1520-0477(2001)082<0247:TNNYRM>2.3.CO;2.

Klotzbach, P., S. Abhik, H. H. Hendon, M. Bell, C. Lucas, A. G. Marshall, and E. C. J. Oliver, 2019: On the emerging relationship between the stratospheric quasi-biennial oscillation and the Madden–Julian oscillation. *Sci. Rep.*, **9**, 2981, https://doi.org/10.1038/s41598-019-40034-6.

Kobayashi, C., H. Endo, Y. Ota, S. Kobayashi, H. Onoda, Y. Harada, K. Onogi, and H. Kamahori, 2014: Preliminary results of the JRA-55C, an atmospheric reanalysis assimilating conventional observations only. *SOLA*, **10**, 78–82, https://doi.org/10.2151/sola.2014-016.

Kobayashi, S., and Coauthors, 2015: The JRA-55 reanalysis: General specifications and basic characteristics. *J. Meteor. Soc. Japan*, **93**, 5–48, https://doi.org/10.2151/jmsj.2015-001.

Lee, J. C. K., and N. P. Klingaman, 2018: The effect of the quasi-biennial oscillation on the Madden–Julian oscillation in the Met Office Unified Model global ocean mixed layer configuration. *Atmos. Sci. Lett.*, **19**, e816, https://doi.org/10.1002/asl.816.

Lim, Y., S.-W. Son, A. G. Marshall, H. H. Hendon, and K.-H. Seo, 2019: Influence of the QBO on MJO prediction skill in the subseasonal-to-seasonal prediction models. *Climate Dyn.*, **53**, 1681–1695, https://doi.org/10.1007/s00382-019-04719-y.

Lin, P., and Q. Fu, 2013: Changes in various branches of the Brewer–Dobson circulation from an ensemble of chemistry climate models. *J. Geophys. Res. Atmos.*, **118**, 73–84, https://doi.org/10.1029/2012JD018813.

——, D. Paynter, Y. Ming, and V. Ramaswamy, 2017: Changes of the tropical tropopause layer under global warming. *J. Climate*, **30**, 1245–1258, https://doi.org/10.1175/JCLI-D-16-0457.1.

Madden, R. A., and P. R. Julian, 1971: Detection of a 40–50 day oscillation in the zonal wind in the tropical Pacific. *J. Atmos. Sci.*, **28**, 702–708, https://doi.org/10.1175/1520-0469(1971)028<0702:DOADOI>2.0.CO;2.

——, and ——, 1972: Description of global-scale circulation cells in the tropics with a 40–50 day period. *J. Atmos. Sci.*, **29**, 1109–1123, https://doi.org/10.1175/1520-0469(1972)029<1109:DOGSCC>2.0.CO;2.

——, and ——, 1994: Observations of the 40–50-day tropical oscillation—A review. *Mon. Wea. Rev.*, **122**, 814–837, https://doi.org/10.1175/1520-0493(1994)122<0814:OOTDTO>2.0.CO;2.

Marshall, A. G., H. H. Hendon, S.-W. Son, and Y. Lim, 2017: Impact of the quasi-biennial oscillation on predictability of the Madden–Julian oscillation. *Climate Dyn.*, **49**, 1365–1377, https://doi.org/10.1007/s00382-016-3392-0.

Martin, Z., S. Wang, J. Nie, and A. Sobel, 2019: The impact of the QBO on MJO convection in cloud-resolving simulations. *J. Atmos. Sci.*, **76**, 669–688, https://doi.org/10.1175/JAS-D-18-0179.1.

——, F. Vitart, S. Wang, and A. Sobel, 2020: The impact of the stratosphere on the MJO in a forecast model. *J. Geophys. Res. Atmos.*, **125**, e2019JD032106. https://doi.org/10.1029/2019JD032106.

Martineau, P., 2017: S-RIP: Zonal-mean dynamical variables of global atmospheric reanalyses on pressure levels. Centre for

Environmental Data Analysis, accessed 24 July 2020, https://doi.org/10.5285/b241a7f536a244749662360bd7839312.

——, J. Wright, N. Zhu, and M. Fujiwara, 2018: Zonal-mean data set of global atmospheric reanalyses on pressure levels. *Earth Syst. Sci. Data*, **10**, 1925–1941, https://doi.org/10.5194/essd-10-1925-2018.

Mayer, K. J., and E. A. Barnes, 2020: Subseasonal midlatitude prediction skill following quasi-biennial oscillation and Madden–Julian Oscillation activity. *Wea. Climate Dyn. Discuss.*, **1**, 247–259, https://doi.org/10.5194/wcd-2019-13.

Mundhenk, B. D., E. A. Barnes, E. D. Maloney, and C. F. Baggett, 2018: Skillful empirical subseasonal prediction of landfalling atmospheric river activity using the Madden–Julian oscillation and quasi-biennial oscillation. *npj Climate Atmos. Sci.*, **1**, 20177, https://doi.org/10.1038/s41612-017-0008-2.

Naito, Y., and S. Yoden, 2006: Behavior of planetary waves before and after stratospheric sudden warming events in several phases of the equatorial QBO. *J. Atmos. Sci.*, **63**, 1637–1649, https://doi.org/10.1175/JAS3702.1.

Neu, J. L., T. Flury, G. L. Manney, M. L. Santee, N. J. Livesey, and J. Worden, 2014: Tropospheric ozone variations governed by changes in stratospheric circulation. *Nat. Geosci.*, **7**, 340–344, https://doi.org/10.1038/ngeo2138.

Nie, J., and A. H. Sobel, 2015: Responses of tropical deep convection to the QBO: Cloud-resolving simulations. *J. Atmos. Sci.*, **72**, 3625–3638, https://doi.org/10.1175/JAS-D-15-0035.1.

Nishimoto, E., and S. Yoden, 2017: Influence of the stratospheric quasi-biennial oscillation on the Madden–Julian oscillation during austral summer. *J. Atmos. Sci.*, **74**, 1105–1125, https://doi.org/10.1175/JAS-D-16-0205.1.

Niwano, M., K. Yamazaki, and M. Shiotani, 2003: Seasonal and QBO variations of ascent rate in the tropical lower stratosphere as inferred from UARS HALOE trace gas data. *J. Geophys. Res.*, **108**, 4794, https://doi.org/10.1029/2003JD003871.

O'Sullivan, D., and R. Young, 1992: Modeling the quasi-biennial oscillation's effect on the winter stratospheric circulation. *J. Atmos. Sci.*, **49**, 2437–2448, https://doi.org/10.1175/1520-0469(1992)049<2437:MTQBOE>2.0.CO;2.

Pascoe, C. L., L. J. Gray, and A. A. Scaife, 2006: A GCM study of the influence of equatorial winds on the timing of sudden stratospheric warmings. *Geophys. Res. Lett.*, **33**, L06825, https://doi.org/10.1029/2005GL024715.

Peña-Ortiz, C., P. Ribera, R. García-Herrera, M. A. Giorgetta, and R. R. García, 2008: Forcing mechanism of the seasonally asymmetric quasi-biennial oscillation secondary circulation in ERA-40 and MAECHAM5. *J. Geophys. Res.*, **113**, D16103, https://doi.org/10.1029/2007JD009288.

Rajendran, K., I. M. Moroz, P. L. Read, and S. M. Osprey, 2016: Synchronisation of the equatorial QBO by the annual cycle in tropical upwelling in a warming climate. *Quart. J. Roy. Meteor. Soc.*, **142**, 1111–1120, https://doi.org/10.1002/qj.2714.

Randel, W. J., and E. J. Jensen, 2013: Physical processes in the tropical tropopause layer and their roles in a changing climate. *Nat. Geosci.*, **6**, 169–176, https://doi.org/10.1038/ngeo1733.

Rao, J., Y. Yu, D. Guo, C. Shi, D. Chen, and D. Hu, 2019: Evaluating the Brewer–Dobson circulation and its responses to ENSO, QBO, and the solar cycle in different reanalyses. *Earth Planet. Phys.*, **3**, 166–181, https://doi.org/10.26464/epp2019012.

Salby, M. L., 1996: *Fundamentals of Atmospheric Physics*. Elsevier, 627 pp.

Son, S., and S. Lee, 2007: Intraseasonal variability of the zonal-mean tropical tropopause height. *J. Atmos. Sci.*, **64**, 2695–2706, https://doi.org/10.1175/JAS3982A.1.

——, Y. Lim, C. Yoo, H. H. Hendon, and J. Kim, 2017: Stratospheric control of the Madden–Julian oscillation. *J. Climate*, **30**, 1909–1922, https://doi.org/10.1175/JCLI-D-16-0620.1.

Tegtmeier, S., and Coauthors, 2020: Temperature and tropopause characteristics from reanalyses data in the tropical tropopause layer. *Atmos. Chem. Phys.*, **20**, 753–770, https://doi.org/10.5194/acp-20-753-2020.

Toms, B. A., E. A. Barnes, E. D. Maloney, and S. C. van den Heever, 2020: The global teleconnection signature of the Madden–Julian oscillation and its modulation by the quasi-biennial oscillation. *J. Geophys. Res. Atmos.*, **125**, e2020JD032653, https://doi.org/10.1029/2020JD032653.

Virts, K. S., and J. M. Wallace, 2014: Observations of temperature, wind, cirrus, and trace gases in the tropical tropopause transition layer during the MJO. *J. Atmos. Sci.*, **71**, 1143–1157, https://doi.org/10.1175/JAS-D-13-0178.1.

Wang, S., M. K. Tippett, A. H. Sobel, Z. Martin, and F. Vitart, 2019: Impact of the QBO on prediction and predictability of the MJO convection. *J. Geophys. Res. Atmos.*, **124**, 11 766–11 782, https://doi.org/10.1029/2019JD030575.

Watson, P. A. G., and L. J. Gray, 2014: How does the quasi-biennial oscillation affect the stratospheric polar vortex? *J. Atmos. Sci.*, **71**, 391–409, https://doi.org/10.1175/JAS-D-13-096.1.

Wheeler, M. C., and H. H. Hendon, 2004: An all-season real-time multivariate MJO index: Development of an index for monitoring and prediction. *Mon. Wea. Rev.*, **132**, 1917–1932, https://doi.org/10.1175/1520-0493(2004)132<1917:AARMMI>2.0.CO;2.

White, I. P., H. Lu, N. J. Mitchell, and T. Phillips, 2015: Dynamical response to the QBO in the northern winter stratosphere: Signatures in wave forcing and eddy fluxes of potential vorticity. *J. Atmos. Sci.*, **72**, 4487–4507, https://doi.org/10.1175/JAS-D-14-0358.1.

Yoo, C., and S.-W. Son, 2016: Modulation of the boreal wintertime Madden–Julian oscillation by the stratospheric quasi-biennial oscillation. *Geophys. Res. Lett.*, **43**, 1392–1398, https://doi.org/10.1002/2016GL067762.

Zhang, C., 2005: Madden–Julian Oscillation. *Rev. Geophys.*, **43**, RG2003, https://doi.org/10.1029/2004RG000158.